β_2-Microglobulin Amyloid Fragment Organization and Morphology and Its Comparison to Aβ Suggests That Amyloid Aggregation Pathways Are Sequence Specific†

Jie Zheng,*,‡ Hyunbum Jang,§ and Ruth Nussinov*,§,||

Department of Chemical and Biomolecular Engineering, The University of Akron, Akron, Ohio 44325, Basic Research Program, SAIC-Frederick, Incorporated Center for Cancer Research, Nanobiology Program, NCI-Frederick, Frederick, Maryland 21702, and Sackler Institute of Molecular Medicine, Department of Human Genetics and Molecular Medicine, Sackler School of Medicine, Tel Aviv University, Tel Aviv 69978, Israel

Received September 20, 2007; Revised Manuscript Received December 13, 2007

ABSTRACT: β_2-Microglobulin (β_2-m) can form dialysis-related amyloid deposits. The structure of a fragment of β_2-m (K3, Ser20-Lys41) in the oligomeric state has recently been solved. We modeled equilibrium structures of K3 oligomers with different organizations (single and double layers) and morphologies (linear-like and annular-like) for the wild-type and mutants using all-atom molecular dynamics (MD) simulations. We focused on the sheet-to-sheet association force, which is the key in the amyloid organization and morphology. For the linear-like morphology, we observed two stable organizations: (i) single-layered parallel-stranded β-sheets and (ii) double-layered parallel-stranded antiparallel β-sheets stacked perpendicular to the fibril axis through the hydrophobic N-terminal−N-terminal (NN) interface. No stable annular structures were observed. The structural instability of the annular morphology was mainly attributed to electrostatic repulsion of three negatively charged residues (Asp15, Glu17, and Asp19) projecting from the same β-strand surface. Linear-like and annular-like double-layered oligomers with the NN interface are energetically more favorable than other oligomers with C-terminal−C-terminal (CC) or C-terminal−N-terminal (CN) interfaces, emphasizing the importance of hydrophobic interactions and side-chain packing in stabilizing these oligomers. Moreover, only linear-like structures, rather than annular structures, with parallel β-strands and antiparallel β-sheet arrangements are possible intermediate states for the K3 β_2-m amyloid fibrils in solution. Comparing the β_2-m fragment with Aβ indicates that while both adopt similar β-strand−turn−β-strand motifs, the final amyloid structures can be dramatically different in size, structure, and morphology due to differences in side-chain packing arrangements, intermolecular driving forces, sequence composition, and residue positions, suggesting that the mechanism leading to distinct morphologies and the aggregation pathways is sequence specific.

Proteins can fold into their unique three-dimensional (3-D) structures to perform their biological functions or they can misfold to form insoluble amyloid fibrils. The fibrils are highly ordered protein aggregates currently known to be associated with ~20 neurodegenerative diseases (*1*). All amyloid fibrils are characterized by a common core structure of cross β-sheets, although these amyloid-forming proteins differ in size, function, sequence, and native structures. There is increasing evidence that the primary toxic species are the soluble prefibrillar intermediates rather than the insoluble mature fibrils (*2*, *3*). These prefibrillar intermediates display various discrete morphologies (micelle-like, annular-like, and linear-like structures) as observed by atomic force microscopy (AFM) and electron microscopy (EM) when exposed to different environmental conditions (*4*−*6*), suggesting that fibrillization may proceed through multiple assembly pathways. However, obtaining atomic-level structures of the amyloid intermediates is still an extremely challenging task due to their small size and dynamic, short-lived nature (*7*, *8*). In parallel, molecular modeling has been widely used to predict the 3-D structure and organization of amyloid oligomers (*9*, *10*), to monitor the kinetics of the aggregation process (*7*, *11*, *12*), to examine the structural stability of the oligomers (*7*, *13*−*17*), and to investigate the interaction of the oligomers with the cell membranes (*18*) at the atomic and coarse-grained levels with explicit and implicit solvent models.

The β_2-microglobulin (β_2-m) protein, a 99-residue protein, is a light chain of the class I major histocompatibility complex (MHC-1) in human and other vertebrates, belonging to the immunoglobulin superfamily (*19*). The dissociation of β_2-m from MHC-1 leads to the subsequent self-assembly

† This work was supported in part by start-up funds (J.Z.) from The University of Akron. This project was funded in whole or in part with Federal funds from the National Cancer Institute, National Institutes of Health (NIH), under Contract NO1-CO-12400. This research was supported (in part) by the Intramural Research Program of the NIH, National Cancer Institute, Center for Cancer Research.

* Corresponding authors. (J.Z.) E-mail: zhengj@uakron.edu; tel.: (330) 972-2096; fax: (330) 972-5856. (R.N.) E-mail: ruthn@ncifcrf.gov; tel.: (301) 846-5579; fax: (301) 846-5598.

‡ The University of Akron.

§ NCI-Frederick.

|| Tel Aviv University.

10.1021/bi7019194 CCC: $40.75
Published on Web 01/24/2008

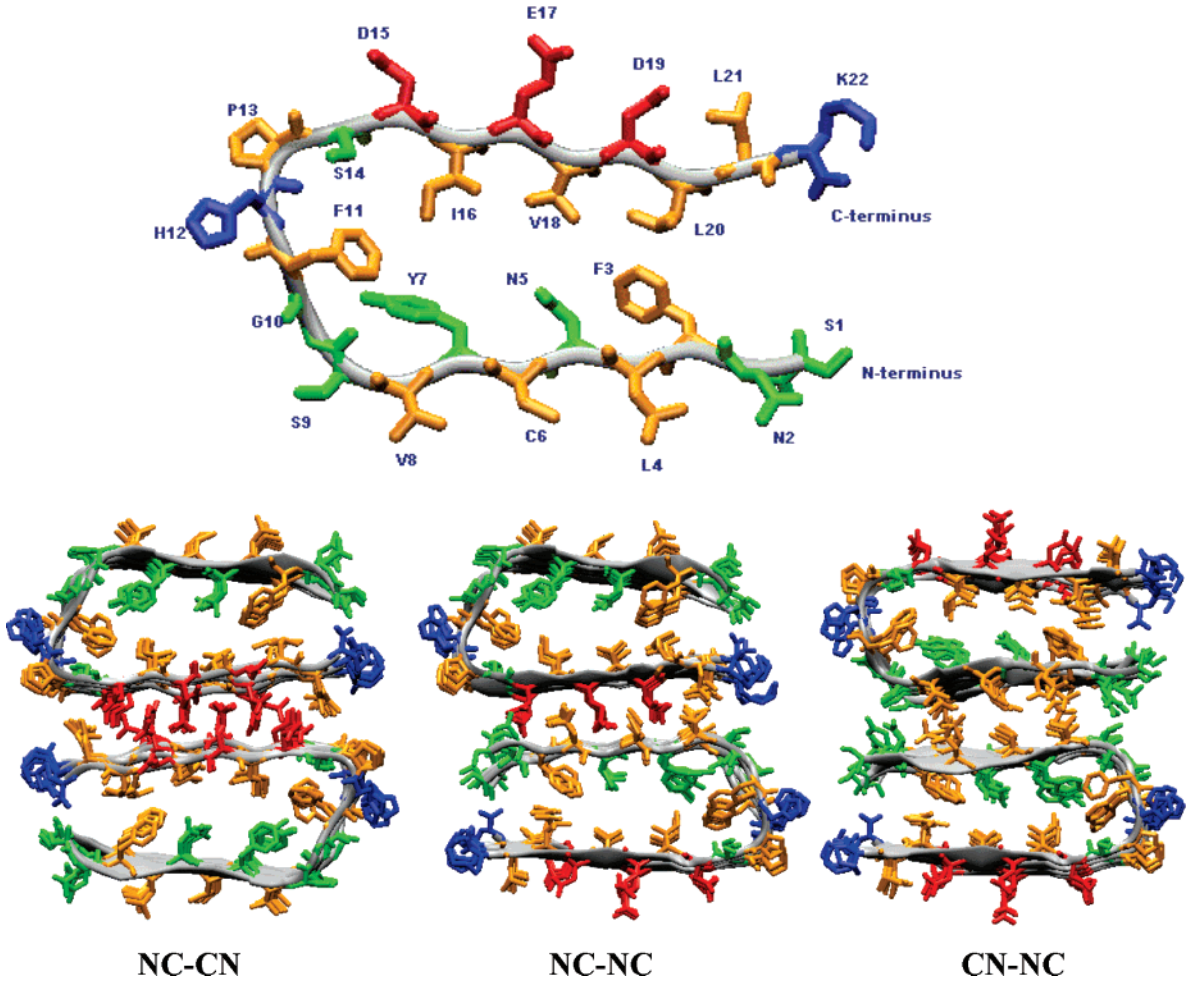

FIGURE 1: Single K3 peptide labeled with residue names (upper panel). Cross-sections of the double-layered K3 10-mers comprising two antiparallel packed pentamers, with the NC−CN, NC−NC, and CN−NC interfaces (lower panel) viewed down the plane of the paper. Color ID: polar residues in green, nonpolar residues in orange, positively charged residues in blue, and negatively charged residues in red. N is the N-terminal strand of the K3 peptide, and C stands for the C-terminal strand. Thus, for example, NC−CN implies that two monomers interact via their C-terminal strands. Here, two pentamers interact with each other.

of the intact wild-type protein into amyloid fibrils (*4*). This is the origin of a serious disease in patients with long-standing uremia and hemodialysis treatment (*20*). The β_2-m protein has been extensively studied as a model system for understanding the relationship between protein folding and amyloid formation. Using AFM and EM, Radford and co-workers (*4*, *21*, *22*) observed that a β_2-m fragment (residues Asp59 to Thr71) formed amyloid fibrils with distinct morphologies (worm-like, rod-like, and long-straight fibrils) in vitro under different solution conditions. Eisenberg and co-workers (*23*) identified a 28-residue fragment of β_2-m (residues Pro72 to Met99) at the C-terminus as an amyloid-forming peptide. Using combined solid-state NMR, X-ray fiber diffraction, and AFM, Goto and co-workers (*24*) recently obtained the 3-D structure of a 22-residue peptide (K3) derived from β_2-m (residues Ser20 to Lys41). They found that the K3 peptide adopted a U-shaped β-strand−turn−β-strand motif, with the K3 molecules stacked in a parallel and staggered fashion to form bent β-sheets. These studies indicate that different β_2-m fragments can aggregate into fibrils, suggesting that fibril formation and the corresponding driving force depend on the sequence composition and residue position (*25*). Within the same region of the same protein, small elements of the primary sequence can initiate distinct intermolecular recognition events that drive the formation of different amyloid structures (*26*).

In this work, we studied the oligomeric states of the K3 peptide in solution with multiple distinct sizes and morphologies. MD simulations were used to explore the structural stability, hydration, and dynamics of these β_2-m oligomers. Protofibrils or fibrils not only grow in the fibril axis direction but also stack in the lateral direction normal to the fibril axis. Fibril growth and stacking are mutually competitive in these two directions: Fibril growth corresponds to intra-sheet interactions, while fibril stacking corresponds to inter-sheet interactions. We consider three different interfaces that can form in the lateral direction upon sheet−sheet association (perpendicular to the fibril axis): As shown in Figure 1, the C-terminal−C-terminal (NC−CN) interface involves strong repulsive electrostatic interactions due to three negatively charged residues at the C-terminal strand; on the other hand, the N-terminal−N-terminal (CN−NC) interface mainly involves hydrophobic interactions arising from maximal contacts between hydrophobic residues along the extended peptide chains. The C-terminal−N-terminal (NC−NC) interface involves both electrostatic and hydrophobic interactions. Since different interfaces between two β-sheets present different interactions via a variety of residues of different

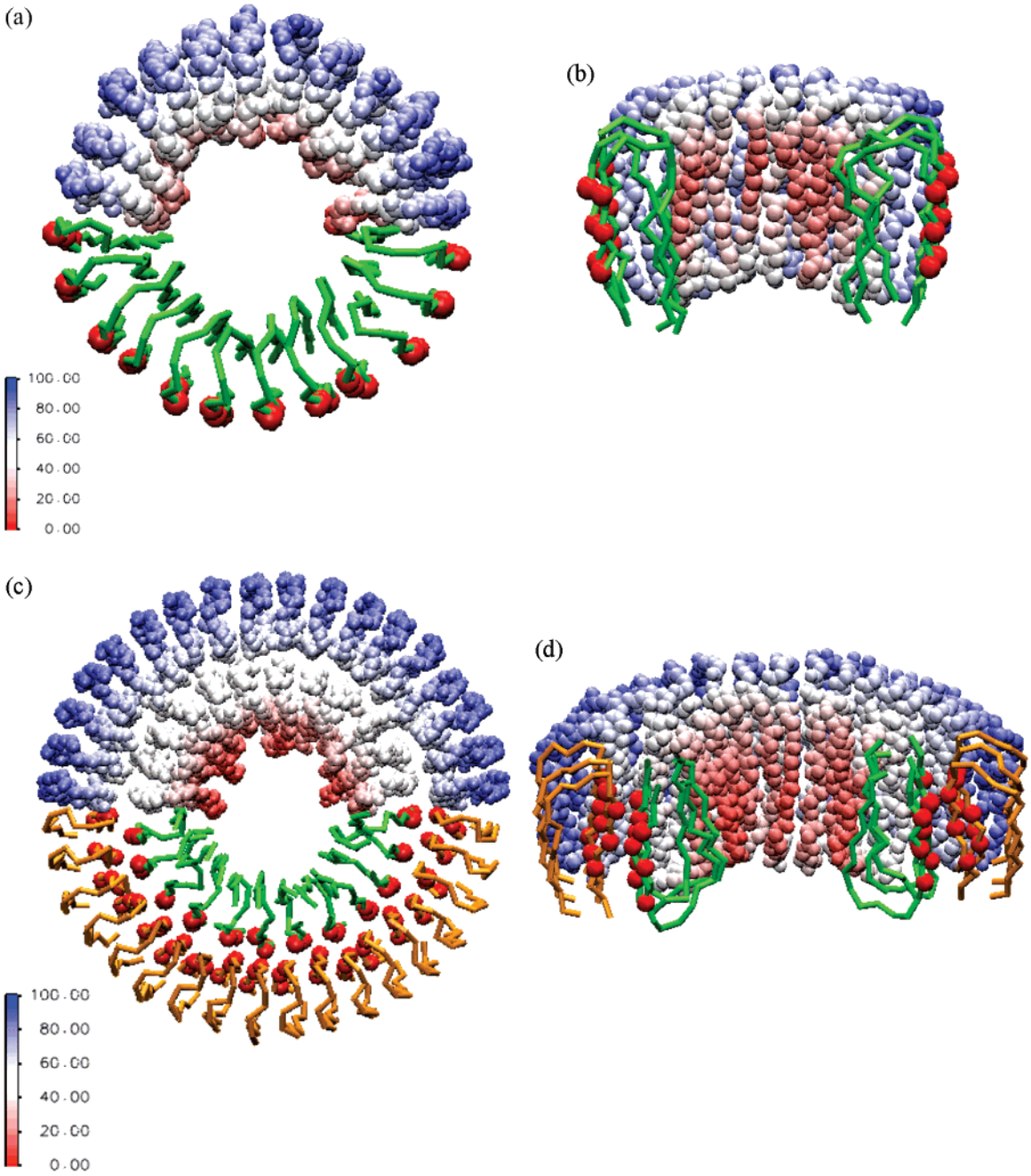

FIGURE 2: Initial single-layered CN annular organization comprising 24 peptides: (a) top view of the whole structure and (b) side view of a cross-section. Initial double-layered NC−CN annular organizations comprising a total 60 peptides (24 peptides in the inner layer and 36 peptides in the outer layer). (c) Top view of the whole structure and (d) side view of a cross-section of two antiparallel β-sheets. The color scale bar indicates the distance of atoms from the center. Three negatively charged residues of Asp15, Glu17, and Asp19 at the C-terminus are presented by red ball-and-stick format to guide the eye in identifying the various interfaces. All images are generated by VMD (*45*).

sizes, hydrophobicities, and side-chain orientations, we examined the effect of these interfaces on the structural stability and morphology of K3 oligomers in solution. Finally, comparison with Aβ, whose monomers in the oligomeric state similarly adopt the β-strand−turn−β-strand motif, suggests that the molecular mechanism leading to distinct morphologies and the aggregation pathways are sequence specific.

MATERIALS AND METHODS

Linear-like Structures. The initial 10 configurations of the β_2-microglobulin fragment (residues 22−41) were derived from solid-state NMR coordinates, which were kindly provided by Goto et al. (*24*). Similar to the Aβ_{40} and Aβ_{42} peptides, a K3 peptide has a U-turn shape consisting of two antiparallel β-strands connected by one loop, β(Ser1-Ser9)−loop(Gly10-Pro13)−β(Ser14-Lys22), as shown in Figure 1. For double-layered models, two β-sheets comprised of five monomeric peptides in each sheet were oriented antiparallel to each other, with an initial separation distance of ~10 Å, while adjacent peptides within a layer were packed parallel to each other, with a separation distance of ~4.7 Å (Figure 1). K3 oligomers can associate through various interfaces (NC−CN, NC−NC, and CN−NC interfaces) in the lateral direction perpendicular to the fibril growth axis. The interfaces between two neighboring β-sheets were generated

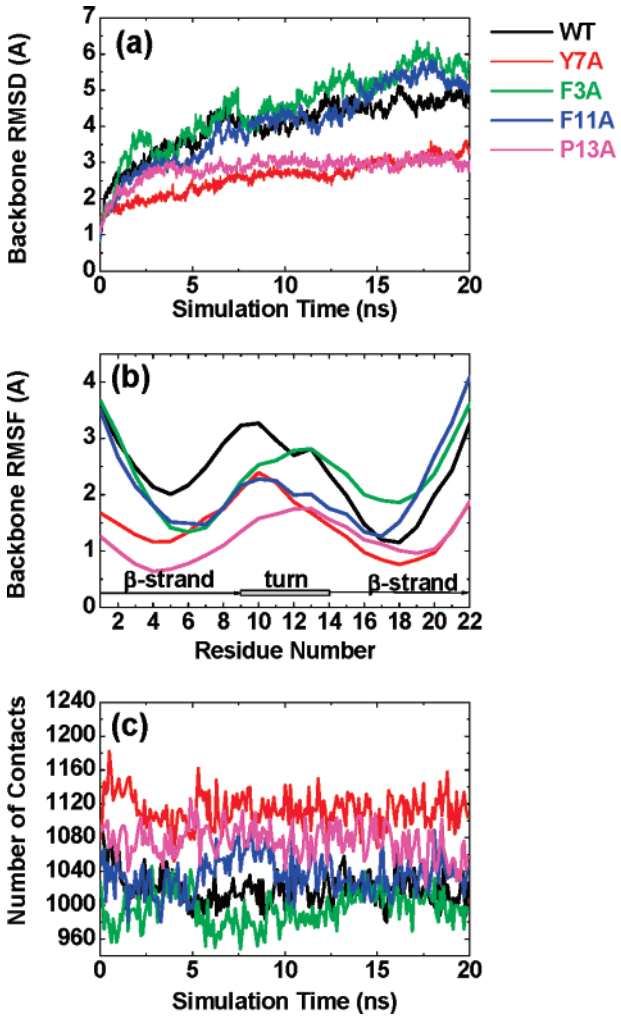

FIGURE 3: Conformational drift and structural flexibility of single-layered linear-like K3 models for the wild-type and mutated sequences. (a) Evolution of backbone rmsds relative to their initial energy-minimized structures, (b) backbone rmsfs relative to the average structures from the last 5 ns of MD trajectories, and (c) the number of native contacts between adjacent peptides.

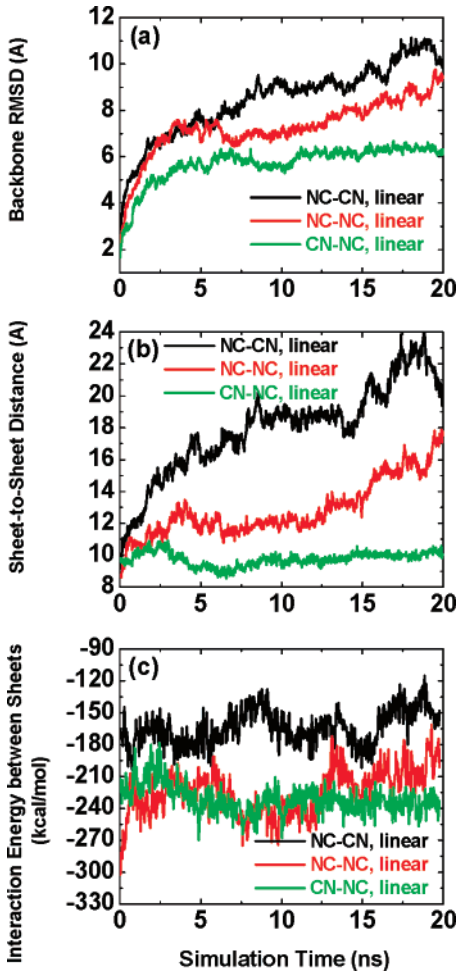

FIGURE 4: Structural and energetic analysis of double-layered linear-like K3 models with different interfaces (i.e., NC−CN, NC−NC, and CN−NC). The time evolution of (a) backbone rmsds relative to their initial energy-minimized structures, (b) averaged mass-center-distances between two facing β-sheets, and (c) interaction energies between two facing β-sheets.

to maximize the overlap of the highly hydrophobic region (Leu4 to Val8) for the CN−NC interface; a highly charged region (Asp15 to Asp19) for the NC−CN interface; and a combination of hydrophobic (Leu4 to Val8) and charged (Asp15 to Asp19) regions for the NC−NC interface. For single-layered organizations comprised of 10 peptides, mutations of aromatic and proline residues were performed (Phe3→Ala, Tyr7→Ala, Phe11→Ala, and Pro13→Ala) to examine the effect of π-stacking on the stability of the preformed oligomers. All initial mutant structures were built by replacing the side chains of the targeted residues without changing the backbone conformations and side-chain orientations. The structure of a designed mutant was first minimized for 500 steps using the steepest decent algorithm with the backbone of the protein restrained before being subjected to the following system setup and production runs.

Annular-like Structure. To build a single-layered annular structure, we first aligned the β-strands of a single peptide to the *z*-axis. Then, the peptide was replicated and translated at a radius distance of *R* from the center, and every replicated peptide was also rotated such that one of the β-strands was facing the *z*-axis of the annular structure. Because of the circular curvature, the inner and outer distances between two neighboring peptides were about 4.2 and 5.6 Å, respectively. The same procedure was used to build a double-layered annular structure with a separation distance of ~9 Å between two layers. Single-layered annular oligomers were comprised of 24 monomeric units with initial inner diameters of ~20 Å, while double-layered annular oligomers consisted of 36 peptides in the outer layer and 24 peptides in the inner layer with initial inner diameters of ~20 Å. In Figure 2, we present typical initial structures of single- and double-layered annular structures. The cross-sections of the double-layered models were well-protected from solvent.

Simulation Protocol. All molecular dynamics simulations were performed using the NAMD program (*27*) with the CHARMM22 force field (*28*). The K3 oligomers and their mutants were solvated with a TIP3P water box with a minimum distance of 10 Å from any edge of the box to any peptide atom. Counterions were added to the box by randomly replacing water molecules to neutralize the system with an ionic concentration of ~0.15 M NaCl. We followed a standard protocol for each MD simulation, which consists of initial minimization, heating procedure, equilibrium, and production run. Each system was initially energy minimized using the conjugate gradient method for 5000 steps with the peptides constrained and an additional 5000 steps without

Table 1: Twist Angles for the Linear-like Models

simulation	twist angle (deg) sheet 1	sheet 2
Linear-like, single-layer		
WT	12.6 ± 1.4	
F3A	16.7 ± 1.4	
Y7A	8.2 ± 1.0	
F11A	12.2 ± 1.7	
P13A	7.0 ± 1.1	
Linear-like, double-layers		
NC−CN	31.2 ± 3.6	39.7 ± 9.4
NC−NC	33.1 ± 5.3	36.0 ± 5.0
CN−NC	12.5 ± 1.3	15.3 ± 2.5

position constraints. The system was then subjected to 500 ps of the heating procedure with the backbone atoms of the peptides constrained to allow for the relaxation of water and ions, followed by a 5000 ps equilibrium run without position constraints. The production simulation used the velocity verlet integrator with an NPT ensemble under periodic boundary conditions with minimum image convention. A constant pressure (1 atm) and temperature (330 K) of the system were maintained by an isotropic Langevin barostat and a Langevin thermostat. Short-range van der Waals interactions employed a switch function with a twin range cutoff of 10.0 and 12.0 Å. Long-range electrostatic interactions employed particle mesh Ewald summation with a grid size of ~1 Å. An integration time step of 2 fs was used, with a multiple time-stepping algorithm employed to compute covalent bonds every time step, short-range nonbonded interactions every two time steps, and long-range electrostatic forces every four time steps. Each system was simulated for 20 ns, and trajectories were saved at 2.0 ps intervals for the analysis. All linear-like models with the same starting structures but different random seeds for initial Maxwell−Boltzman distribution of velocities were performed to validate simulation data. No significant differences in the results were found for the use of different initial velocities (rmsd and rmsf profiles for single-layered linear-like structures and rmsd and separation distance between two adjacent layers for double-layered linear-like structures). These latter validation simulations entailed eight additional MD simulations, which were run for a total of 160 ns.

Analysis Details. (i) The relative structural stability and conformational change of the oligomers was measured by root-mean-squared deviation (rmsd) of the backbone atoms with respect to the initial minimized experimental structure throughout the simulations.

(ii) The root-mean-squared atomic fluctuations (rmsf) were calculated for each individual residue by aligning all trajectory structures with the averaged structure from the trajectory. The overall size of a given structure is measured by its radius of gyration (R_g). R_g is defined as the mass-weighted geometric mean of the distance of each atom from the protein's center of mass

$$R_g = \sqrt{\sum_{i=1}^{n} m_i (r_i - r_{com})^2 / \sum_{i=1}^{n} m_i}$$

(iii) The intra-sheet interactions are indicated by native contacts consisting of backbone hydrogen bonds and side-chain contacts. A hydrogen bond is assigned if the distance between donor D and acceptor A is ≤3.6 Å and the angle D−H···A is ≥120°; a side-chain contact is defined if the distance between the center of mass of two adjacent sidechains is less than 6.7 Å.

Table 2: Averaged Interaction Energies and Sc between Two β-Sheets for All Double-Layered Organizations, Including Linear and Annular Structures[a]

simulation	interaction energy (kcal/mol)	Sc
Linear structure		
NC−CN	−162.3 ± 17.0	0.43 ± 0.10
NC−NC	−216.3 ± 20.7	0.55 ± 0.06
CN−NC	−234.8 ± 9.8	0.61 ± 0.05
Annular structure		
^{out}CN−NC^{in}	−1082.3 ± 28.5	0.65 ± 0.01
^{out}NC−CN^{in}	−536.5 ± 42.7	0.57 ± 0.02
^{out}NC−NC^{in}	−850.1 ± 42.0	0.60 ± 0.02
^{out}CN−CN^{in}	−893.8 ± 28.3	0.59 ± 0.02

[a] Mean interaction energy and Sc are averaged from the last 10 ns simulations.

(iv) The shape complementarity (Sc) is used to measure the geometric surface complementarity of protein−protein interfaces between two adjacent layers, where 1.0 represents a perfect match between the interfaces, while 0.0 represents two unrelated interfaces. Sc is calculated by using the program SC of CCP4 with default parameters (*29*).

(v) Dimeric structures were extracted from the explicit MD trajectories by excluding water molecules at 10 ps time intervals. Each structure was first subjected to energy minimization for 1000 conjugate gradient steps. At the minimized state, the solvation energy was calculated using the Generalized Born method with a simple switching method (GBSW) (*30*, *31*). Thus, the interaction energy between two dimeric structures was calculated by

$$\langle \Delta G_{dimer} \rangle = E^{mm}_{dimer} + G^{gbsw}_{dimer} - (E^{mm}_{monomer1} + G^{gbsw}_{monomer1}) - (E^{mm}_{monomer2} + G^{gbsw}_{monomer2})$$

RESULTS AND DISCUSSION

Overall Behavior of the Linear-like Structures. The backbone rmsd profiles for the single-layered linear oligomers (Figure 3a) showed that Pro13Ala and Tyr7Ala mutants have lower structural deviations than the wild-type, while Phe3Ala and Phe11Ala mutants experienced structural deviations comparable to the wild-type. Since the K3 peptide has a high content of aromatic residues, it appears that the disruption of aromatic stacking via single-point mutations has an inconsistent effect on the equilibrium state of preformed oligomers, resulting from local structural arrangements (i.e., optimal side-chain packing and steric effects). Figure 3b shows the residue-based rmsfs of the mutants as compared to the wild-type. The Tyr7Ala and Pro13Ala mutants with relatively small magnitude of residue fluctuations displayed small rmsd structural derivations. To further characterize the inter-strand interactions within a single-layered structure, we measured the native contacts between all adjacent K3 peptides. As seen in Figure 3c, the Tyr7Ala and Pro13Ala mutants have much higher native contacts (i.e., backbone−backbone H-bonds and side-chain−side-chain contacts) than the other mutants and the wild-type. The stabilization is due to the increase not only in the side-chain−

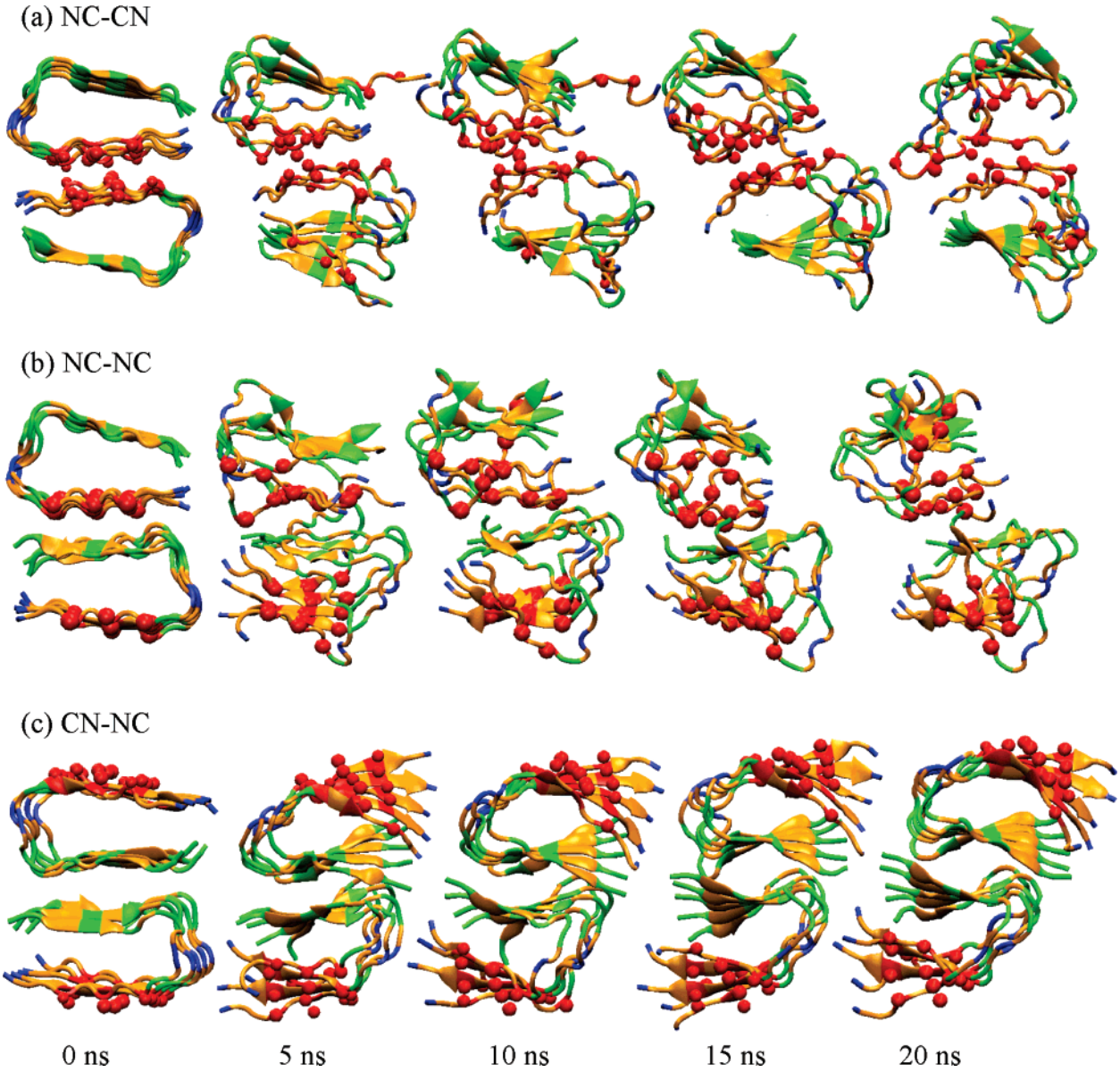

FIGURE 5: Snapshots from MD simulations for double-layered linear-like K3 models with the (a) NC−CN, (b) NC−NC, and (c) CN−NC interfaces at 0, 5, 10, 15, and 20 ns. The color coding is the same as in Figure 1. Three negatively charged residues of Asp15, Glu17, and Asp19 at the C-terminus are presented by red ball-and-stick format to guide the eye for identifying the various interfaces.

side-chain contacts but also in the backbone−backbone hydrogen bonds. Furthermore, Tyr7 and Pro13 were packed against their neighboring aromatic residues of Phe11 and His12, respectively, with similar side-chain orientations (Figure 1). Substitution by the smaller sized Ala at the Tyr7 or Pro13 positions would allow for adjustment of the conformation to avoid steric conflicts induced by original side-chain packing, while still maintaining a favorable interaction. This result confirms that more stable structures can be obtained by increasing the contacts between peptide interfaces and lowering residue fluctuations in local secondary structures.

The rmsf also showed that residues in the turn region exhibited a higher flexibility than those in the β-strand regions, except for residues near the N-/C-termini that were exposed to the solvent (Figure 3b). Visual inspection of all trajectories of the mutants and the wild-type showed that all 10-mer structures were still able to maintain the β-strand−turn−β-strand motif without disassociation of the β-strands, indicating that mutations (Phe3, Tyr7, Phe11, and Pro13) did not alter significantly the 10-mer structure.

We assessed the possibility of two preformed β-sheets associated in the lateral direction by considering three distinct interfaces in double-layered linear oligomers. For two β-sheets with an antiparallel arrangement, the CN−NC interface consisted of highly hydrophobic patches of Leu4, Cys6, and Val8; the NC−CN interface mainly consisted of negatively charged residues of Asp15, Glu17, and Asp19; and the NC−NC interface consisted of the combination of hydrophobic and negatively charged residues. Backbone rmsd profiles (Figure 4a) showed that a double-layered oligomer with the CN−NC interface exhibited a higher structural stability than the other two oligomers with the NC−NC and NC−CN interfaces, in which the rmsd value for the CN−NC oligomer reached a plateau of ~6 Å, while the NC−CN and NC−NC oligomers displayed their instability with continuously increased rmsds within the 20 ns simulations. We looked into the geometrical match of side chains that

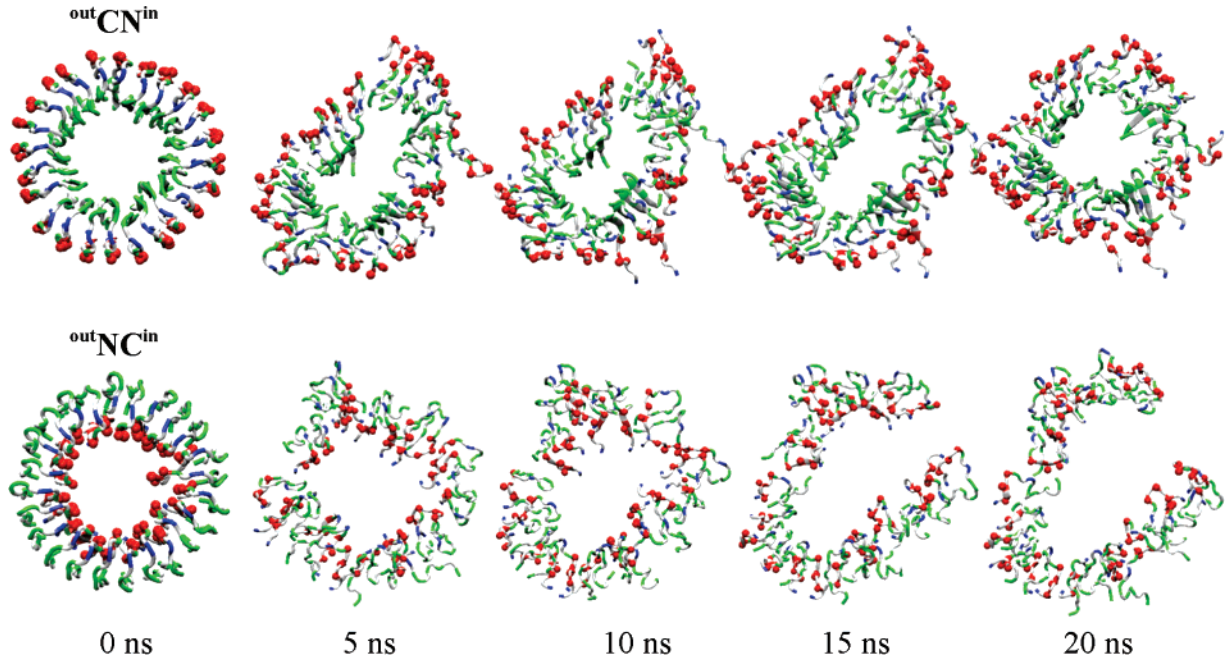

FIGURE 6: Snapshots from MD simulations for the single-layered (a) $^{out}CN^{in}$ and (b) $^{out}NC^{in}$ annular structures at 0, 5, 10, 15, and 20 ns. Superscripts of out and in indicate which terminus faces to the solvent and to the pore, respectively. Three negatively charged residues of Asp15, Glu17, and Asp19 at the C-terminus are presented by red ball-and-stick format to guide eyes for identifying interfaces. Neither of the annular structures is able to maintain the initial annular shape within 20 ns.

protrude from the two antiparallel β-sheets stacked against each other using a Sc parameter (*29*). The results are shown in Table 2. The CN−NC interface had the highest Sc value of 0.61, indicating that the side chains at the interface were more comfortable in interacting with each other, without any unfavorable steric effects. On the other hand, Sc values were largely reduced to 0.43 for the NC−CN interface due to charge repulsion and to 0.55 for the NC−NC interface due to weak hydrophobic interactions. We further analyzed the interaction energies between the two β-sheets with various interfaces (Figure 4c and Table 2). Energy profiles showed that the CN−NC oligomer (−234.8 kcal/mol) was energetically more favorable than the NC−NC (−216.3 kcal/mol) and NC−CN (−162.3 kcal/mol) oligomers, suggesting that different surface packings were stabilized by different forces. These data are well-correlated with the previous analysis of the rmsd, sheet-to-sheet distance, and Sc.

Visual inspection of the snapshots along the simulation trajectories (Figure 5) also illustrated that the CN−NC oligomer was able to retain its packing very close to the initial antiparallel organization in the lateral direction, with a sheet-to-sheet distance of 10 Å (Figure 4b) and no disruption of the secondary structure of the strand−turn−strand motif, although the β-strands were twisted by 10° relative to each other (Table 1). In contrast, the oligomers with the NC−CN and NC−NC interfaces exhibited disturbed packing and secondary structures. In the cases of the NC−CN interface, the two β-sheets moved away from each other after 2 ns (Figures 4b and 5), largely due to repulsive electrostatic interactions induced by Asp15, Glu17, and Asp19 located at the interface. The NC−NC interface also displayed an unstable structure. Although repulsive charge interactions at the interface were attenuated, they still cannot compensate for the loss of hydrophobic interactions, highlighting the important role of hydrophobic interactions in the association of K3 peptides.

Combining the information of the relative structural deviation (rmsd), geometrical characterization (sheet-to-sheet distance and Sc), visual inspection (snapshots), and interaction energy, it is clear that the CN−NC oligomer is the most stable structure, while the NC−CN and NC−NC oligomers suffer from structural instability. This indicates that when two linear-like β-sheets of the K3 peptides stack in the lateral direction in solution, they exclusively associate through the CN−NC interface, while the other two sheet−sheet associations via the NC−NC and NC−CN interfaces are eliminated due to structural instability. We emphasize that short MD simulations are insufficient to provide absolute conformational stabilities; thus, the disaggregation of the most stable CN−NC interface found in this study might be a slow kinetic process that cannot be fully explored within the 20 ns time scale. However, it is a necessary condition that the proposed oligomeric models remain organized within the period of simulation time. If they do not, then the models would be unviable for further propagation of the fiber growth.

Overall Behavior of the Annular-like Structures. We examined the structural stability and dynamics of two single-layered annular structures in solution. Each structure consisted of 24 peptides, with an initial inner diameter of 20 Å. As shown in Figure 6, when the highly negatively charged C-terminal strands faced the bulk solvent, the whole structure quickly lost its initial circular shape at 5 ns, and the pore size reduced at 10 ns. Interestingly, at 20 ns, the structure tended to reorganize back to a circular shape but with four separated linear-like subunits. In contrast, when the hydrophobic N-terminus faced the bulk solvent, the structure was unable to maintain the closed-circular shape and ruptured, opening widely at 20 ns. This could be due to both repulsive forces induced by the negatively charged residues from the inside and unfavorable hydrophobic−water interactions from the outside. Both the rmsd and the radius of gyration profiles (Figure 7) were consistent with the visual inspection of the

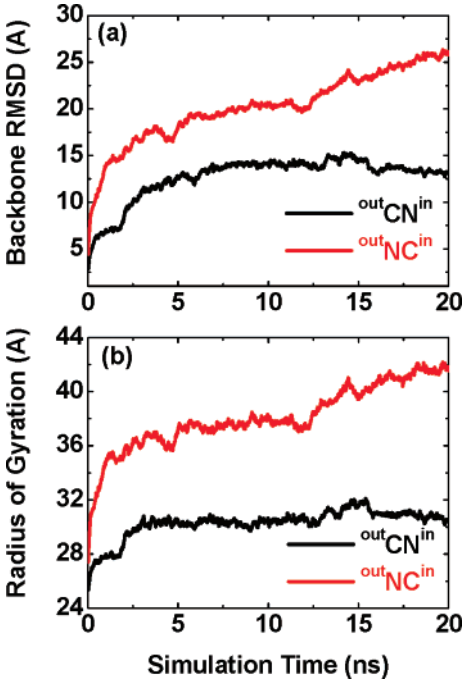

FIGURE 7: Structural analysis of single-layered annular structures. Time evolution of (a) backbone rmsds and (b) radius of gyrations, relative to their initial energy-minimized structures. Superscripts of out and in indicate which terminus faces the solvent and the pore, respectively.

snapshots from the simulations. While both single-layered annular structures displayed structural instability in solution, they experienced different instability scenarios: one tended to collapse and the other widely opened.

Since single-layered annular structures were unstable in solution, we constructed and explored double-layered annular structures with various interfaces at the inner and outer circular layers. Backbone rmsd profiles (Figure 8a) showed that as compared to the NC−CN and NC−NC annular structures, the CN−NC and CN−CN annular structures have relatively lower structural deviations. The radius of gyration (R_g) was used to measure the overall size (outer diameter) of the annular structures. The NC−CN and NC−NC structures had similar R_g values of ∼46 Å at 20 ns, while the CN−NC and CN−CN structures had relatively larger R_g values of ∼51 Å at 20 ns, consistent with the trend observed in the rmsds (Figure 8b). Visual inspection of the snapshots (Figure 9) showed that all double-layered annular structures experienced structural instability. The instability of the annular structures was mainly due to the three neighboring charged residues (Asp15, Glu17, and Asp19) at one β-strand region of the C-terminus. Since all charged residues are parallel, aligned in an in-register manner ∼5 Å apart within the β-sheet, no matter whether these negatively charged residues face the bulk or the pore solvent, or embed at the interface, strong intermolecular electrostatic repulsion tends to push the peptides away from each other. The repulsion force will overwhelm the stabilizing effect of the hydrophobic side-chain contacts, leading to a tendency to open the annular structure. This effect becomes more pronounced in the case of the NC−CN structure, where pairwise repulsive electrostatic interactions between the C-terminus−C-terminus of the inner and outer layers tend to push the two layers away. Moreover, unfavorable hydrophobic−water interactions would tend to unfold the structures at the outer layer or to collapse at the inner layer, when hydrophobic residues at the N-terminus face the bulk or pore solvent. All those effects lead to a structural instability of the double-layered K3 annular structures in solution.

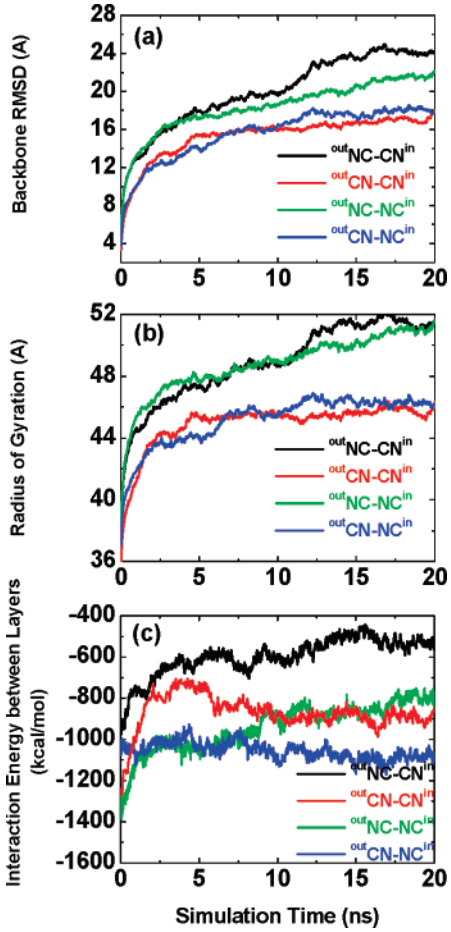

FIGURE 8: Structural and energetic analysis of double-layered annular-like K3 models with different interfaces (i.e., ^{out}NC−CN^{in}, ^{out}CN−CN^{in}, ^{out}NC−NC^{in}, and ^{out}CN−NC^{in}). Superscripts of out and in indicate which terminus faces the solvent and which the pore, respectively. (a) Backbone rmsds relative to their initial energy-minimized structures, (b) radius of gyrations relative to their initial energy-minimized structures; and (c) interaction energies between two facing β-sheets as a function of time.

The interaction energies between two layers (Figure 8c and Table 2) were evaluated by the GBSW method (*30*, *31*) in the CHARMM program. The CN−NC structure had a much stronger interaction energy than other structures, and the energy differences between different structures ranged from −188.5 to −545.8 kcal/mol. These are qualitatively consistent with the Sc results (Table 2). This highlights the important role of hydrophobic interactions in the association force, as well as side-chain packing (Sc). For the linear-like structures, it is expected that with the increase in the number of peptides, the oligomer stability increases dramatically, especially when the number of peptides is smaller than the minimal nucleus seed (*13*, *32*, *33*). However, the increasing number of K3 peptides should have a minor effect on the stability enhancement of annular structures because strong electrostatic repulsive forces induced by Asp15, Glu17, and Asp19 in the same β-strands can easily disrupt the circular curvature. We should note that all simulation models

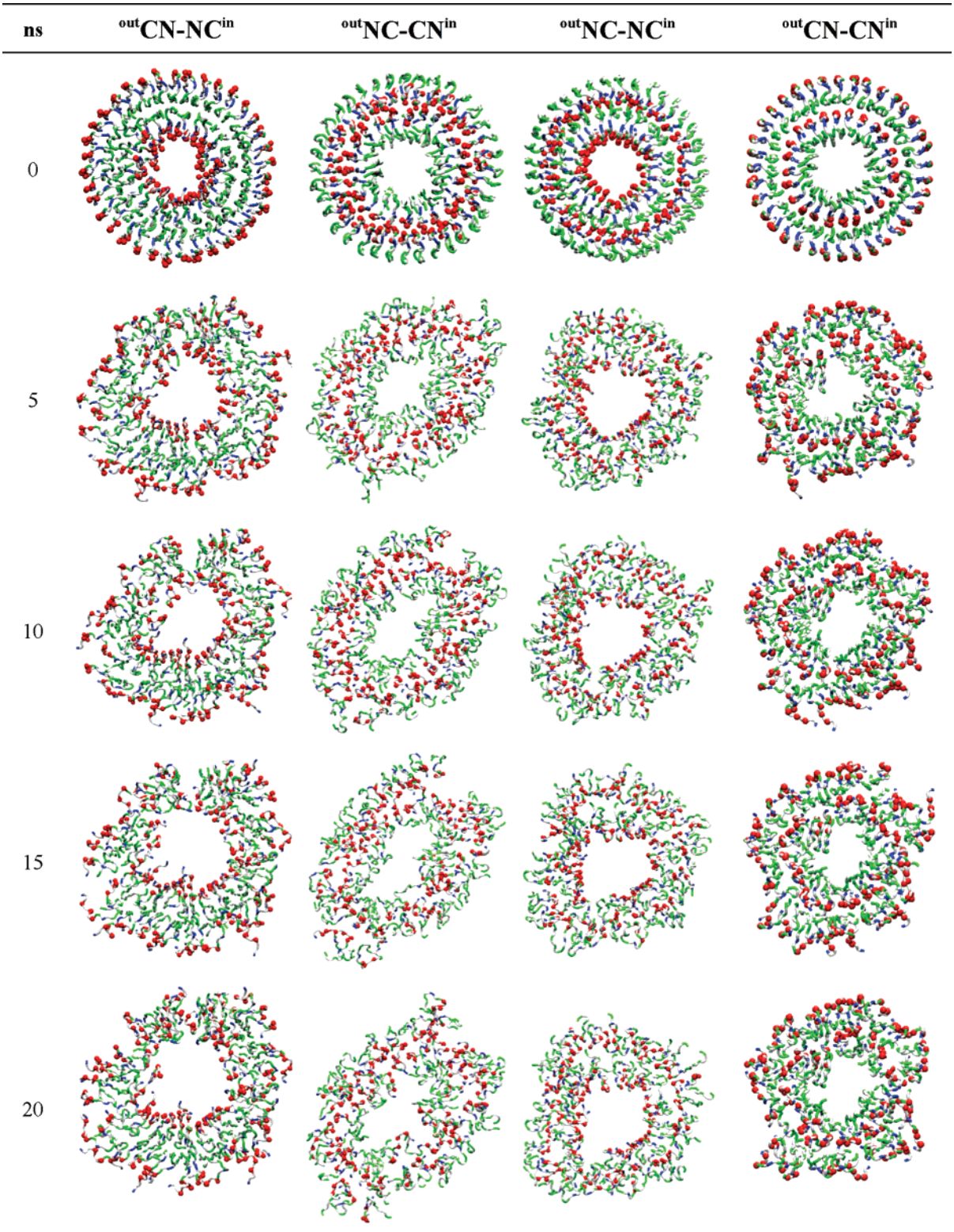

FIGURE 9: Snapshots from MD simulations for the double-layered annular structures with different interfaces (i.e., ^{out}NC−CN^{in}, ^{out}CN−CN^{in}, ^{out}NC−NC^{in}, and ^{out}CN−NC^{in}) at 0, 5, 10, 15, and 20 ns. Superscripts of out and in indicate which terminus faces the solvent and which faces the pore, respectively. Three negatively charged residues of Asp15, Glu17, and Asp19 at the C-terminus are presented by red ball-and-stick format to guide the eye for identifying the interfaces. None of the annular structures is able to maintain the initial annular shape within 20 ns.

proposed here are constructed in an in-register way, in which the structures were packed in a way as to obtain large side-chain contacts at the sheet−sheet interface between two adjacent β-sheets matching each other perfectly without steric overlaps. Although all K3 annular structures experienced a high structural instability, we cannot exclude the possibility of other intermolecular registration of the chains. For example, models with out-of-register chains will reduce both the destabilizing electrostatic repulsive forces and the stabilizing intermolecular contacts. To explore the stability

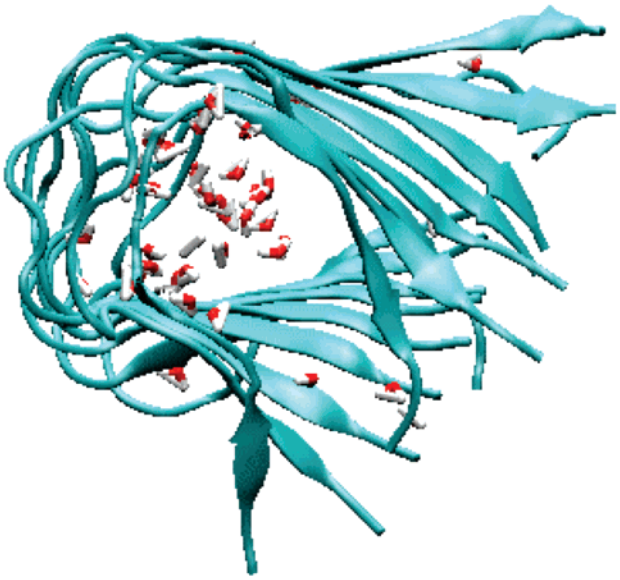

FIGURE 10: Representative cross-section of the interior hydration of the single-layered linear-like model, viewed along the protofibrils axis. Water molecules are trapped in the interior cavity near the loop region.

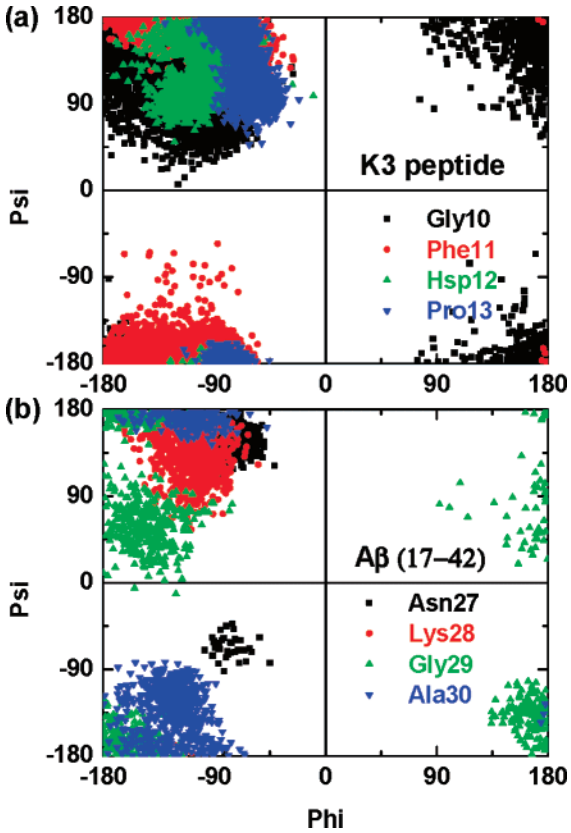

FIGURE 11: Backbone torsion angle (φ, ψ) distributions for the loop residues in the (a) K3 and (b) Aβ_{17-42} peptides. PDB code of Aβ_{17-42} is 2beg (*43*).

of K3 oligomers with alternate possible out-of-register chains, additional MD simulations will be required. Here, all single- and double-layered annular structures exhibited structural instability, indicating that annular structures of K3 peptides are unlikely to serve as intermediates for protofibril formation in solution.

β-Strand−Turn−β-Strand Motif in the Preformed Oligomers Is Stabilized by Intramolecular Interactions. Similar to the K3 peptide (residues 20−41) of β_2-m, Nishino and co-workers (*34*) also reported that a peptide fragment (residues 21−31) of β_2-m can form a bent hairpin-like structure, highlighting the essential region of residues 20−41 in amyloid fibril formation. Moreover, a number of amyloidogenic peptides including Aβ (*35*) and human CA150 (*36*) displayed the common secondary structural motif of β-strand−turn−β-strand, which is formed by two antiparallel β-strands linked by a flexible turn. The two β-strand segments form two separate in-register parallel β-sheets, where main-chain hydrogen bonding occurs between neighboring β-strands in the direction of the fibril axis. The net bend angle of 180° brings the two β-sheets in contact through side-chain−side-chain interactions (*37*). As compared to an extended conformation, the β-strand−turn−β-strand motif induces more tightly packed residues in a limited space, leading to more intramolecular interactions via hydrophobic interactions, hydrogen bonds, steric zippers, or salt bridges, which are absent in a single sheet. Thus, the β-strand−turn−β-strand motif has an inherent ability to stabilize itself through those buried side-chain−side-chain interactions. For instance, the human CA150 peptide has a buried salt bridge between Glu7 and Arg24 (*36*) providing additional contribution to structural stability, similar to the buried salt bridge between Asp23 and Lys28 in the Aβ peptide (*9*, *35*). The β-strand−turn−β-strand motif offers two opposite faces for lateral associations through N-/C-terminal β-strands. Proline mutagenesis of Aβ_{42} suggested that the formation of a turn structure could play a crucial role in its aggregation ability and neurotoxicity (*38*, *39*). Wu and co-workers (*40*) also reported that a strand−turn−strand structure could be an important binding intermediate for Aβ fibril growth. In addition, this U-bent hairpin motif is large enough to accommodate small molecules such as waters and ions in the cavity (Figure 10). Penetrating water molecules inside the cavity form hydrogen bonds with buried side chains. These hydrogen bonds not only increase the desolvation barrier of the cavity structure but also help maintain and stabilize this structure due to the desolvation penalty (*41*). Therefore, a turn-induced motif is advantageous, as it may lead to a zipper motif resembling the tightly packed β-sheets of shorter peptides.

Comparison to Aβ Peptides. It is interesting to compare the structure of Aβ fibrils with that of K3 fibrils. Aβ peptides have been studied extensively by experiments and computations. Tycko and co-workers (*42*) proposed a quaternary structural model of the Aβ_{1-40} protofibrils using solid-state NMR, while Riek and co-workers (*43*) proposed a model for Aβ_{17-42} protofibrils using the combination of hydrogen-/deuterium-exchange NMR data, side-chain packing constraints from pairwise mutagenesis, solid-state NMR, and EM. In parallel, using simulations, Ma and Nussinov (*9*) independently proposed another model for the Aβ (Aβ_{16-35}) using computational modeling. All three models have a similar β-hairpin motif (i.e., β-strand−turn−β-strand motif) with the same side-chain orientation but with a distinct turn structure. We recently performed MD simulations to study the structural organization of Aβ_{17-42} with different sizes, structures, and morphologies (*44*), obtaining results similar to Hummer and Buchete (*15*).

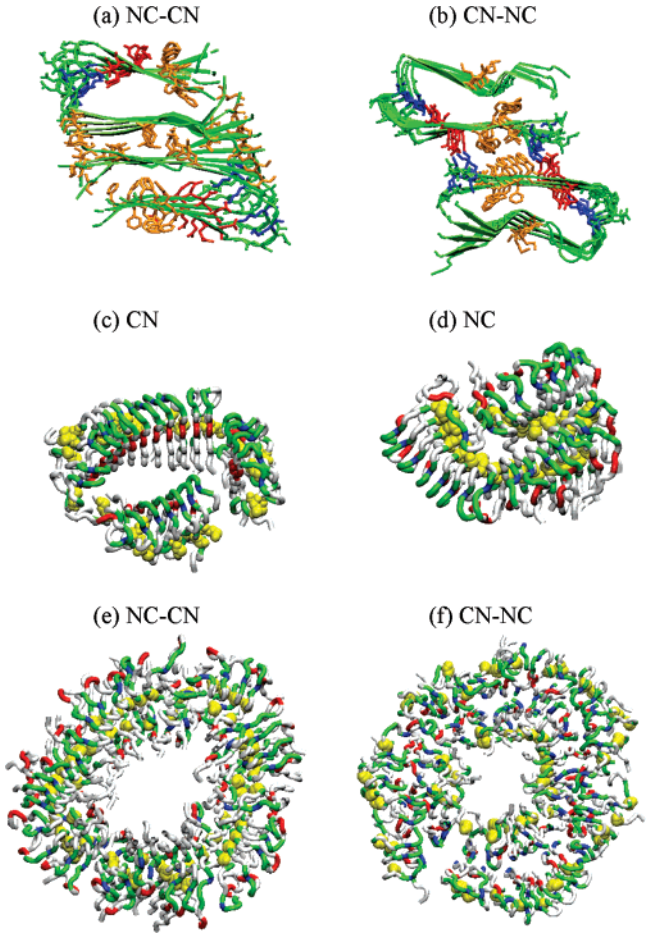

FIGURE 12: Snapshots from MD simulations for the Aβ models. (a) Double-layered linear structure with NC−CN interface at 20 ns, (b) double-layered linear structure with CN−NC interface at 20 ns, (c) single-layered annular CN structure where the hydrophobic C-terminal faces the bulk solvent at 20 ns, (d) single-layered annular NC structure where the hydrophilic N-terminal faces the bulk solvent at 20 ns, (e) double-layered annular structure with NC−CN interface at 50 ns, and (f) double-layered annular structure with CN−NC interface at 50 ns. For the annular structures, residues at position 35 are presented by yellow ball-and-sticks to guide the eye for identifying the interface.

Similar to the K3 peptide, the Aβ peptide has a U-bent shape. Figure 11 shows the distribution of the main-chain dihedral angles of the loop residues in both K3 and Aβ peptides. It can be seen that the K3 and Aβ peptides have similar (φ, ψ) distributions at the β-turn regions, although their sequences are different. Moreover, the U-shaped motif of K3 creates a hydrophobic cavity with a diameter of 6−7 Å similar to Aβ peptides, allowing water molecules and ions to conduct through. Both Aβ and K3 oligomers are characterized by twist angles ranging from 7 to 17° between neighboring β-strands. Because of the character of the β-strand−turn−β-strand motif, Aβ peptides can associate with each other in the lateral direction through different β-strand interfaces. In the linear-like organization, Aβ oligomers with the NC−CN interface, stabilized by hydrophobic and van der Waals interactions, are energetically more favorable than those with the CN−NC interface stabilized by hydrophobic interactions and salt bridges. However, both interfaces exhibit a high structural stability (Figure 12a,b). This indicates that the Aβ peptides can be stacked on top of each other with multiple layers in the lateral direction; that is, the Aβ peptides can form multiple layers through either the NC−CN or the CN−NC interface. In contrast, K3 peptides can associate two β-sheets only through the CN−NC interface. Further, the K3 peptides cannot form stable annular structures, no matter whether they are single-layered or double-layered. On the other hand, Aβ peptides can form a stable double-layered annular structure with the NC−CN interface (Figure 12e), although other Aβ annular models display structural instability. For example, the single-layered CN annular oligomer with the C-terminus facing the bulk solvent finally broke down into three subunits consisting of twisted linear-like oligomers (Figure 12c), while the annular NC oligomer with the N-terminal facing bulk solvent collapsed within 20 ns due to strong hydrophobic interactions between the inner C-terminal residues (Figure 12d). Interestingly, although both single-layered structures exhibited severe structural deformation, they displayed different oligomerization scenarios: one structure broke down into pieces and the other collapsed. The CN−NC annular structure experienced large twisting motions with many opening/closing events at the outer layer during the simulations (Figure 12f). The structural comparison of K3 peptides with Aβ peptides reveals that although different primary amyloidgenic sequences could fold into similar monomeric motifs (the β-strand−turn−β-strand motif in this case), when assembling these motifs into highly ordered aggregates, the final stable amyloid structures can be dramatically different in size, structure, and morphology due to the difference in the geometrical side-chain packing arrangements, intermolecular driving forces, and primary sequence compositions and positions, suggesting that the molecular mechanism leading to distinct morphologies and the corresponding aggregation pathways is sequence specific.

CONCLUSION

We explored the stability and dynamics of K3 peptides with different structures, sizes, and morphologies in solution using MD simulations. For the linear-like structures, the stable ordered aggregates of the K3 peptide are (i) single-layered oligomers with a parallel orientation within the sheets and (ii) double-layered CN−NC oligomers with a parallel orientation within the sheets and antiparallel organization between the sheets. The parallel β-strand arrangement is favored in energy due to side-chain interactions mainly from hydrogen bonds between the amide groups and the aromatic π-stacking. The antiparallel β-sheet organization is mainly stabilized by highly hydrophobic interactions. In contrast, all annular-like oligomers, including single- and double-layered structures, displayed structural instability because the circular shape resulted in close contacts of three negatively charged residues (Asp15, Glu17, and Asp19) located at the same C-terminal β-strand, leading to strong repulsive electrostatic interactions. Simulations suggest that linear structures of K3 peptides, instead of annular structures, are possible intermediates in the formation of protofibrils in solution. Of particular interest, comparison with Aβ indicates that while in both cases the monomers adopt the U-turn β-strand−turn−β-strand motif when in the single-layered oligomeric state, the preferred protofibril organizations and morphologies are different. The apparently universal amyloid motif does not necessarily dictate similar aggregation pathways. Different sequences and sizes may mandate

different side-chain packing and intermolecular driving forces, suggesting that the molecular mechanism leading to distinct morphologies and the corresponding aggregation pathways are sequence specific.

ACKNOWLEDGMENT

We thank Dr. Buyong Ma for helpful discussions. This study utilized the high-performance computational capabilities of the Biowulf PC/Linux cluster at the National Institutes of Health, Bethesda, MD (http://biowulf.nih.gov). We also thank the Frederick Advanced Biomedical Computing Center for computational facilities used in this work. The content of this publication does not necessarily reflect the views or policies of the Department of Health and Human Services, nor does mention of trade names, commercial products, or organizations imply endorsement by the U.S. Government.

SUPPORTING INFORMATION AVAILABLE

The rmsd and rmsf profiles for single-layered linear-like structures and rmsd and separation distances between two adjacent layers for double-layered linear-like structures. This material is available free of charge via the Internet at http://pubs.acs.org.

REFERENCES

1. Meredith, S. C. (2006) Protein denaturation and aggregation. Cellular responses to denatured and aggregated proteins, *Ann. N.Y. Acad. Sci. 1066*, 181−221.
2. Bucciantini, M., Calloni, G., Chiti, F., Formigli, L., Nosi, D., Dobson, C. M., and Stefani, M. (2004) Prefibrillar amyloid protein aggregates share common features of cytotoxicity, *J. Biol. Chem. 279*, 31374−31382.
3. Lashuel, H. A., and Lansbury, P. T. (2006) Are amyloid diseases caused by protein aggregates that mimic bacterial pore-forming toxins? *Q. Rev. Biophys. 39*, 167−201.
4. Gosal, W. S., Morten, I. J., Hewitt, E. W., Smith, D. A., Thomson, N. H., and Radford, S. E. (2005) Competing pathways determine fibril morphology in the self-assembly of [β]2-microglobulin into amyloid, *J. Mol. Biol. 351*, 850−864.
5. Lashuel, H. A., Hartley, D., Petre, B. M., Walz, T., and Lansbury, P. T. (2002) Amyloid pores from pathogenic mutations, *Nature (London, U.K.) 418*, 291.
6. Lashuel, H. A., Petre, B. M., Wall, J., Simon, M., Nowak, R. J., Walz, T., and Lansbury, J. P. T. (2002) α-Synuclein, especially the Parkinson's disease-associated mutants, forms pore-like annular and tubular protofibrils, *J. Mol. Biol. 322*, 1089−1102.
7. Mousseau, N., and Derreumaux, P. (2005) Exploring the early steps of amyloid peptide aggregation by computers, *Acc. Chem. Res. 38*, 885−891.
8. Makabe, K., McElheny, D., Tereshko, V., Hilyard, A., Gawlak, G., Yan, S., Koide, A., and Koide, S. (2006) Atomic structures of peptide self-assembly mimics, *Proc. Natl. Acad. Sci. U.S.A. 103*, 17753−17758.
9. Ma, B., and Nussinov, R. (2002) Stabilities and conformations of Alzheimer's β-amyloid peptide oligomers (Abeta 16−22, Abeta 16−35, and Abeta 10−35): Sequence effects, *Proc. Natl. Acad. Sci. U.S.A. 99*, 14126−14131.
10. Armen, R. S., Bernard, B. M., Day, R., Alonso, D. O. V., and Daggett, V. (2005) Characterization of a possible amyloidogenic precursor in glutamine-repeat neurodegenerative diseases, *Proc. Natl. Acad. Sci. U.S.A. 102*, 13433−13438.
11. Nguyen, H. D., and Hall, C. K. (2006) Spontaneous fibril formation by polyalanines: Discontinuous molecular dynamics simulations, *J. Am. Chem. Soc. 128*, 1890−1901.
12. Pellarin, R., and Caflisch, A. (2006) Interpreting the aggregation kinetics of amyloid peptides, *J. Mol. Biol. 360*, 882−892.
13. Zheng, J., Ma, B., Tsai, C.-J., and Nussinov, R. (2006) Structural stability and dynamics of an amyloid-forming peptide GNNQQNY from the yeast prion sup-35, *Biophys. J. 91*, 824−833.
14. Wu, C., Lei, H., and Duan, Y. (2005) Elongation of ordered peptide aggregate of an amyloidogenic hexapeptide NFGAIL observed in molecular dynamics simulations with an explicit solvent, *J. Am. Chem. Soc. 127*, 13530−13537.
15. Buchete, N.-V., and Hummer, G. (2007) Structure and dynamics of parallel {β}-sheets, hydrophobic core, and loops in Alzheimer's A{β} fibrils, *Biophys. J. 92*, 3032−3039.
16. Huet, A., and Derreumaux, P. (2006) Impact of the mutation A21G (Flemish variant) on Alzheimer's {β}-amyloid dimers by molecular dynamics simulations, *Biophys. J. 91*, 3829−3840.
17. Baumketner, A., Bernstein, S. L., Wyttenbach, T., Bitan, G., Teplow, D. B., Bowers, M. T., and Shea, J.-E. (2006) Amyloid β-protein monomer structure: A computational and experimental study, *Protein Sci. 15*, 420−428.
18. Jang, H., Zheng, J., and Nussinov, R. (2007) Models of {β}-amyloid ion-channels in the membrane suggest that channel formation in the bilayer is a dynamic process, *Biophys. J. 93*, 1938−1949.
19. Maenaka, K., and Jones, E. Y. (1999) MHC superfamily structure and the immune system, *Curr. Opin. Struct. Biol. 9*, 745−753.
20. Chen, Y., and Dokholyan, N. V. (2005) A single disulfide bond differentiates aggregation pathways of [β]2-microglobulin, *J. Mol. Biol. 354*, 473−482.
21. Kad, N. M., Thomson, N. H., Smith, D. P., Smith, D. A., and Radford, S. E. (2001) [β]2-Microglobulin and its deamidated variant, N17D, form amyloid fibrils with a range of morphologies in vitro, *J. Mol. Biol. 313*, 559−571.
22. Jones, S., Manning, J., Kad, N. M., and Radford, S. E. (2003) Amyloid-forming peptides from [β]2-microglobulin: Insights into the mechanism of fibril formation in vitro, *J. Mol. Biol. 325*, 249−257.
23. Ivanova, M. I., Gingery, M., Whitson, L. J., and Eisenberg, D. (2003) Role of the C-terminal 28 residues of β-2 microglobulin in amyloid fibril formation, *Biochemistry 42*, 13536−13540.
24. Iwata, K., Fujiwara, T., Matsuki, Y., Akutsu, H., Takahashi, S., Naiki, H., and Goto, Y. (2006) 3-D structure of amyloid protofilaments of β2-microglobulin fragment probed by solid-state NMR, *Proc. Natl. Acad. Sci. U.S.A. 103*, 18119−18124.
25. Ivanova, M. I., Sawaya, M. R., Gingery, M., Attinger, A., and Eisenberg, D. (2004) An amyloid-forming segment of β2-microglobulin suggests a molecular model for the fibril, *Proc. Natl. Acad. Sci. U.S.A. 101*, 10584−10589.
26. Tessier, P. M., and Lindquist, S. (2007) Prion recognition elements govern nucleation, strain specificity, and species barriers, *Nature (London, U.K.) 447*, 556−561.
27. Kale, L., Skeel, R., Bhandarkar, M., Brunner, R., Gursoy, A., Krawetz, N., Phillips, J., Shinozaki, A., Varadarajan, K., and Schulten, K. (1999) NAMD2: Greater scalability for parallel molecular dynamics, *J. Comput. Phys. 151*, 283−312.
28. Brooks, B. R., Bruccoleri, R. E., Olafson, B. D., States, D. J., Swaminathan, S., and Karplus, M. (1983) CHARMM: A program for macromolecular energy, minimization, and dynamics calculations, *J. Comput. Chem. 4*, 187−217.
29. Lawrence, M. C., and Colman, P. M. (1993) Shape complementarity at protein/protein interfaces, *J. Mol. Biol. 234*, 946−950.
30. Im, W., Lee, M. S., and Brooks, C. L., III. (2003) Generalized born model with a simple smoothing function, *J. Comput. Chem. 24*, 1691−1702.
31. Im, W., Feig, M., and Brooks, C. L., III. (2003) An implicit membrane generalized born theory for the study of structure, stability, and interactions of membrane proteins, *Biophys. J. 85*, 2900−2918.
32. Tsai, H.-H., Zanuy, D., Haspel, N., Gunasekaran, K., Ma, B., Tsai, C.-J., and Nussinov, R. (2004) The stability and dynamics of the human calcitonin amyloid peptide DFNKF, *Biophys. J. 87*, 146−158.
33. Zanuy, D., Ma, B., and Nussinov, R. (2003) Short peptide amyloid organization: Stabilities and conformations of the islet amyloid peptide NFGAIL, *Biophys. J. 84*, 1884−1894.
34. Nishino, M., Sugita, Y., Yoda, T., and Okamoto, Y. (2005) Structures of a peptide fragment of [β]2-microglobulin studied by replica-exchange molecular dynamics simulations: Towards the understanding of the mechanism of amyloid formation, *FEBS Lett. 579*, 5425−5429.
35. Petkova, A. T., Ishii, Y., Balbach, J. J., Antzutkin, O. N., Leapman, R. D., Delaglio, F., and Tycko, R. (2002) A structural model for Alzheimer's β-amyloid fibrils based on experimental constraints from solid state NMR, *Proc. Natl. Acad. Sci. U.S.A. 99*, 16742−16747.

36. Ferguson, N., Becker, J., Tidow, H., Tremmel, S., Sharpe, T. D., Krause, G., Flinders, J., Petrovich, M., Berriman, J., Oschkinat, H., and Fersht, A. R. (2006) General structural motifs of amyloid protofilaments, *Proc. Natl. Acad. Sci. U.S.A. 103*, 16248−16253.
37. Naito, A., and Kawamura, I. (2007) Solid-state NMR as a method to reveal structure and membrane interaction of amyloidogenic proteins and peptides, *Biochim. Biophys. Acta 1768*, 1900−1912.
38. Zheng, J., Ma, B., and Nussinov, R. (2006) Consensus features in amyloid fibrils: Sheet−sheet recognition via a (polar or nonpolar) zipper structure, *Phys. Biol. 3*, 1−4.
39. Masuda, Y., Irie, K., Murakami, K., Ohigashi, H., Ohashi, R., Takegoshi, K., Shimizu, T., and Shirasawa, T. (2005) Verification of the turn at positions 22 and 23 of the [β]-amyloid fibrils with Italian mutation using solid-state NMR, *Bioorg. Med. Chem. 13*, 6803−6809.
40. Han, W., and Wu, Y. D. (2005) A strand−loop−strand structure is a possible intermediate in fibril elongation: Long time simulations of amyloid-β peptide (10−35), *J. Am. Chem. Soc. 127*, 15408−15416.
41. Tarus, B., Straub, J. E., and Thirumalai, D. (2006) Dynamics of Asp23−Lys28 salt-bridge formation in A[β]10−35 monomers, *J. Am. Chem. Soc. 128*, 16159−16168.
42. Petkova, A. T., Yau, W. M., and Tycko, R. (2006) Experimental constraints on quaternary structure in Alzheimer's β-amyloid fibrils, *Biochemistry 45*, 498−512.
43. Luhrs, T., Ritter, C., Adrian, M., Riek-Loher, D., Bohrmann, B., Dobeli, H., Schubert, D., and Riek, R. (2005) 3-D structure of Alzheimer's amyloid-{β}(1−42) fibrils, *Proc. Natl. Acad. Sci. U.S.A. 102*, 17342−17347.
44. Zheng, J., Jang, H., Ma, B., Tsai, C.-J., and Nussinov, R. (2007) Modeling the Alzheimer a{β}17−42 fibril architecture: Tight intermolecular sheet−sheet association and intramolecular hydrated cavities, *Biophys. J. 93*, 3046−3057.
45. Humphrey, W., Dalke, A., and Schulten, K. (1996) VMD: Visual molecular dynamics, *J. Mol. Graphics 14*, 33−38.

BI7019194